Acta Crystallographica Section B
Structural Science
ISSN 0108-7681

Neutron Rietveld refinement of the incommensurate phase of the ordered perovskite Pb_2CoWO_6

G. Baldinozzi,[a]* G. Calvarin,[a] Ph. Sciau,[a]† D. Grebille[b] and E. Suard[c]

[a]Structures, propriétés et modélisation des solides, UMR CNRS, Ecole Centrale Paris, 92295 Châtenay Malabry CEDEX, France, [b]CRISMAT, UMR CNRS-ISMRa, 14050 Caen CEDEX, France, and [c]ILL, BP 156, 38042 Grenoble CEDEX 9, France

† Current address: CEMES, UPR CNRS, BP 4347, 31055 Toulouse CEDEX 4, France.

Correspondence e-mail: baldinozzi@cps.ecp.fr

Received 4 June 1999
Accepted 13 January 2000

The incommensurate structure of lead cobalt tungstate has been refined by the Rietveld method on neutron data collected at 250 K. The space group is planar monoclinic $I2/m(\alpha 0\gamma)0s$ [a = 7.9602 (4), b = 5.6779 (3), c = 5.6967 (3) Å, β = 90.047 (5)°, $\mathbf{q}_{inc}$ = 0.9000 (9)$\mathbf{a}^*$ + 0.1735 (6)$\mathbf{c}^*$]. The use of powder diffraction techniques to investigate ferroelastic modulated phases is discussed and compared with a previous polydomain single-crystal structural analysis. The modulated displacements of light atoms have been determined, allowing an accurate description of the modulation of both the cations and the O-atom framework. The refinement suggests a displacive model for the phase transition, involving significant atomic shifts for Pb atoms and a quite complex mixing of tilt and deformation of the oxygen octahedra. The average character of this modulated structure is antiferroelectric.

1. Introduction

The prototype structure of perovskite compounds (ABO_3) consists of corner-sharing oxygen octahedra BO_6 stacked along the three ⟨100⟩ directions. The A cation sits in the cubo-octahedral voids among the octahedra. In Pb_2CoWO_6, the B site, at the octahedron centre, is occupied by two different species of cations: a complex perovskite structure is obtained. Owing to the stoichiometry, and the charge and cationic size differences of Co and W, this structure (called elpasolite) exhibits cationic ordering along ⟨111⟩ directions. Therefore, the space group is cubic $Fm\bar{3}m$, since the simple perovskite lattice parameter is doubled.

Detailed structural understanding of the data is important because not only is it a well studied example of ferroelectrics, but also it is of considerable practical interest. It is the end member of solid solutions with Pb_2YbNbO_6 having applications as high-density capacitors, electromechanical transducers, dielectric and pyroelectric devices (Lines, 1996).

These physical properties are closely related to an interesting original phase transition sequence involving normal to incommensurate phase transitions (Brixel *et al.*, 1985). In fact, Pb_2CoWO_6 does not present the standard static behaviour: the monoclinic incommensurate phase is stable in a finite range of temperatures (230–298 K; Sciau *et al.*, 1992), but neither a lock-in transition nor a group–subgroup relationship between the incommensurately modulated structure and the lower-temperature phase are observed. A careful structural resolution of the incommensurate phase on a polydomain single crystal was performed recently by Bonin *et al.* (1995). Nevertheless, because of the complex polydomain state of the sample only the main features of the modulated displacements were modeled. The symmetry of the lower-temperature phase

is orthorhombic (Baldinozzi *et al.*, 1993) and the commensurate superstructure appearing at the phase transition corresponds to the mode condensation at two other points of the Brillouin zone (Baldinozzi *et al.*, 1995). This second phase transition (incommensurate–commensurate) presents a large hysteresis (at ∼20 K), possibly related to the pinning of domain wall boundaries by some kind of defect. Apparently, there is no evidence of any influence of the pinning on the amplitude of the modulation vector. On powder samples the phase transition from incommensurate to commensurate is not complete. Finally, an antiferromagnetic phase transition takes place at ∼9 K.

The object of this paper is to contribute to the determination of the complex phenomena related to the onset of the incommensurate structure in Pb_2CoWO_6 and to show that Rietveld refinement of modulated phases can be competitive and often equivalent to the structural resolutions using single-crystal techniques, expecially when no single domain crystal is available for the interesting phase.

2. Experimental

2.1. Synthesis

Powdered samples of Pb_2CoWO_6 were obtained from stoichiometric amounts of high-purity PbO, WO_3 and CoO. These oxides were ground together in a mortar with some alcohol to obtain an intimate mixture. The mixture was then heated in an alumina crucible under a PbO atmosphere at 1050 K for 12 h.

The powders of Pb_2CoWO_6 obtained were well crystallized; examination of the sample by X-ray diffraction in the cubic phase assesses the very good quality of the synthesis. No peak other than the perovskite was observed.

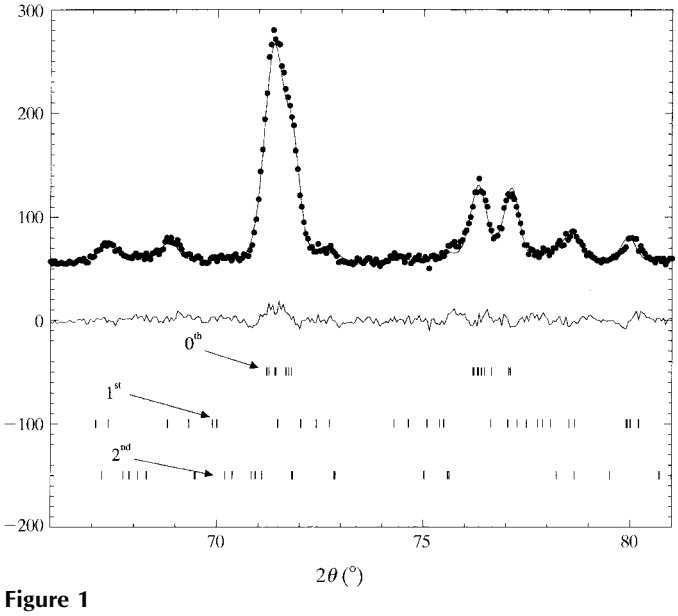

Figure 1
Details of the observed (full dots), calculated and difference (solid lines) neutron diffraction patterns of Pb_2CoWO_6 in the incommensurate phase. The ticks show the contribution of main (zeroth), first- and second-order satellite reflections.

Table 1
Characteristics of the neutron data collection for Pb_2CoWO_6 on a D1a diffractometer at ILL.

	250 K
Wavelength (Å)	1.911
Monochromator	Ge(115)
Step scan width (2θ, °)	0.05
2θ range (°)	10.05–159.45
Monitor	5000
No. of scans	8
Maximum counts	1554
Average background	85
No. *hkl*0	161
No. *hkl*±1	217
No. *hkl*±	202
Molecular weight	753.16
Calculated density	9.712
Space group	$I2/m(\alpha 0\gamma)0s$
α (°)	0.9000 (9)
γ (°)	0.1735 (6)
a (Å)	7.9602 (4)
b (Å)	5.6779 (3)
c (Å)	5.6967 (3)
β (°)	90.047 (5)
R_{wp}	0.0453
R_{exp}	0.0337
S	1.34
R_{F0}	0.0218
R_{F1}	0.0720
R_{F2}	0.1271
$R_{I\,all}$	0.0394

The synthesis of single crystals of Pb_2CoWO_6 has already been described elsewhere (Sun *et al.*, 1991). Platelets for transmission electron microscopy were thinned using an Ar^+-ion beam. These samples were coated on one side with an amorphous carbon film to increase their conductivity. The low-temperature study was performed using a Philips CM20 electron microscope and a Gatan cooling stage.

2.2. Data collection

Neutron data were collected on the high-resolution powder diffractometer D1a at the Institute Laue–Langevin in Grenoble using a monochromatic beam. Powders of the sample were placed in a vanadium canister and loaded into a He cryostat. Data were collected at 250 K. As the data collection was performed using a multicounter detector, the weighting scheme of each point after averaging was calculated paying attention to the multicounter corrections. According to the *International Tables for Crystallography* (Wilson, 1992) the neutron scattering lengths for Pb, W, Co and O are 9.4017, 4.77, 2.50 and 5.803 fm, respectively. The details of data collection are summarized in Table 1.[1]

2.3. Data analysis

The powder diffraction patterns were refined using the Rietveld program *XND* (Version 1.18; Bérar & Garnier, 1992). This program has been modified to handle the refine-

[1] Supplementary data for this paper are available from the IUCr electronic archives (Reference: SH0136). Services for accessing these data are described at the back of the journal.

Table 2
Atomic positions and anisotropic thermal displacement parameters of the average structure (R_{wp} = 0.0666).

Atom	x	y	z	U^{11}	U^{22}	U^{33}	U^{12}	U^{13}	U^{23}
O2	0.0198 (6)	0.2393 (8)	0.2467 (8)	0.024 (2)	0.021 (2)	0.021 (2)	−0.001 (1)	0.002 (1)	−0.006 (1)
O1	0.2369 (8)	0	−0.0377 (7)	0.004 (1)	0.029 (2)	0.023 (2)	0	−0.010 (4)	0
Pb	0.2521 (10)	0	0.4991 (5)	0.024 (2)	0.044 (2)	0.029 (2)	0	−0.003 (3)	0
Co	1/2	0	0	0.020 (7)	−0.023 (8)	0.136 (17)	0	−0.096 (9)	0
W	0	0	0	0.016 (2)	0.025 (3)	−0.030 (6)	0	−0.008 (4)	0

ment of incommensurately modulated phases using the de Wolff formalism (Wilson, 1992).

During the different stages of the refinement of the modulated phase, the four dimensional Fourier series maps were calculated using the refinement package *JANA* (Petříček & Dusek, 1998). The integrated intensities needed as input data were extracted from the powder diffraction pattern using *XND*.

The coefficients of the Fourier expansion of the modulation functions are used as independent parameters in the refinements: the position u_i^μ for the atom μ in the modulated structure along the coordinate i is given by

$$u_i^\mu(\bar{x}_4^\mu) = B_{0i}^\mu + \sum_{n=1}^{\infty}[A_{ni}^\mu \sin(2\pi n\bar{x}_4^\mu) + B_{ni}^\mu \cos(2\pi n\bar{x}_4^\mu)],$$

where $\bar{x}_4^\mu$ is the variable describing the average position of the atom μ in the internal subspace defined by the modulation vector and orthogonal to the euclidean space ($\bar{x}_4^\mu = \mathbf{q}\cdot\mathbf{r}^\mu$, $\mathbf{r}^\mu$ being the average position of this atom).

The restrictions (Table 3) imposed by the site symmetries of the considered Wyckoff positions on the Fourier terms of the atomic modulation functions were found solving the de Wolff equations. Since only first- and second-order satellites are observed (Fig. 1), the refinement parameters for the starting model included only Fourier amplitudes of the first and second order.

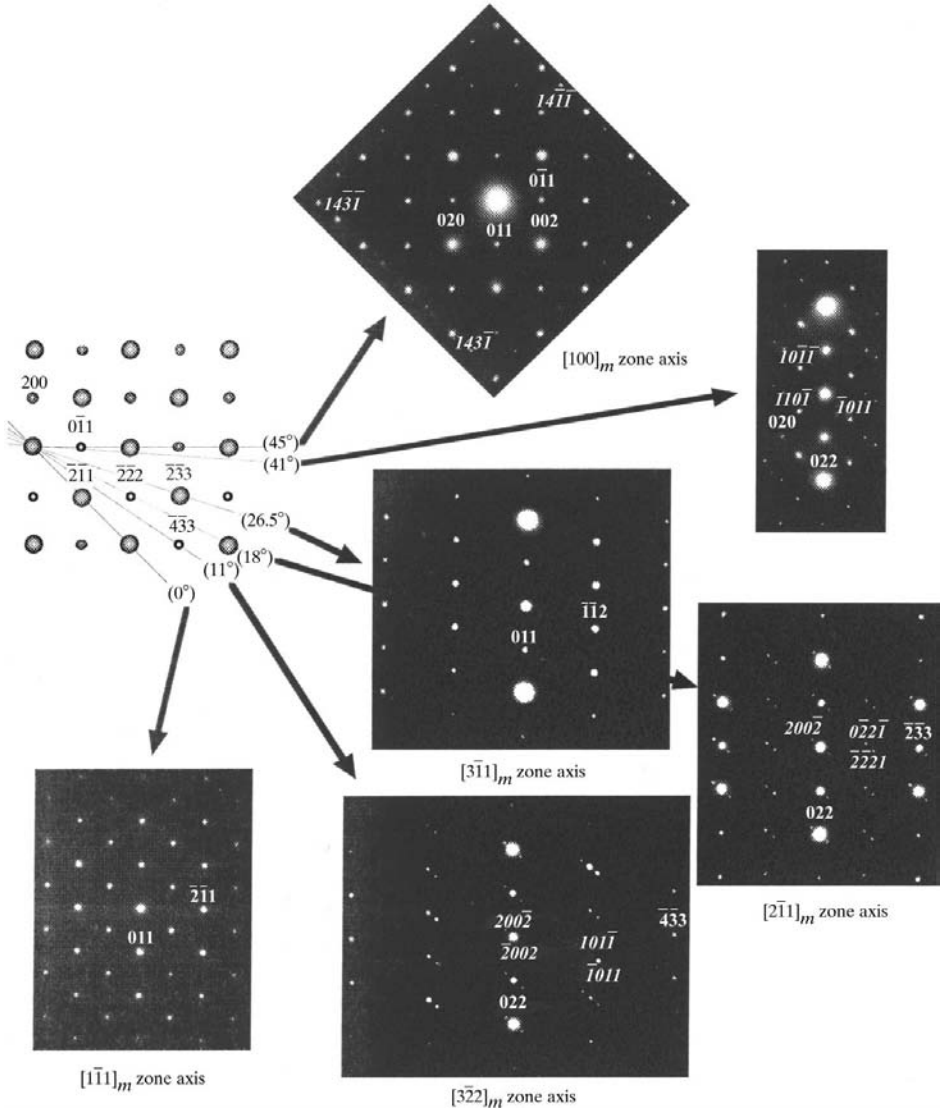

Figure 2
Electron diffraction patterns of Pb_2CoWO_6 in the incommensurate phase obtained by a rotation around $[011]_m$.

3. Results

3.1. Symmetry and structure of the incommensurate phase

A transmission electron microscopy study (Sciau *et al.*, 1990) of a limited number of zone axes has confirmed the mono-incommensurate character of this modulated phase and has allowed the determination of the incommensurate wavevector. These results are confirmed and complemented by the analysis of a larger number of microdiffraction patterns obtained in a single domain with a very small spot size, as displayed in Fig. 2 (a preliminary analysis of the same microscopy plates was reported by Sciau & Grebille, 1994). The satellite spots are observed near the main spots forbidden by the I centring and

Table 3
Atomic displacement and displacive modulation wave constraints in the space group $I2/m(\alpha 0\gamma)0s$.

Atom	Site symmetry	B_0	A_1	B_1	A_2	B_2
O2	1	–	–	–	–	–
Pb, O1	m_s	$y = 0$	$A_{1x} = A_{1z} = 0$	$B_{1x} = B_{1z} = 0$	$A_{2y} = 0$	$B_{2y} = 0$
Co	$2/m_s$	$x = \frac{1}{2}, y = z = 0$	$A_{1x} = A_{1z} = 0$	$B_{1x} = B_{1y} = B_{1z} = 0$	$A_{2y} = 0$	$B_{2x} = B_{2y} = B_{2z} = 0$
W	$2/m_s$	$x = y = z = 0$	$A_{1x} = A_{1z} = 0$	$B_{1x} = B_{1y} = B_{1z} = 0$	$A_{2y} = 0$	$B_{2x} = B_{2y} = B_{2z} = 0$

can be indexed by a modulation vector $\mathbf{q}_{\rm inc} = \alpha\mathbf{a}^* + \gamma\mathbf{c}^*$, where $\alpha \sim 9/10$ and $\gamma \sim 3/17$. The analysis of systematic extinctions in the $[010]_m$ zone axis presented in Fig. 3 definitely suggests the existence of an m_s symmetry (four-dimensional glide plane), since only second-order satellites are observed. Therefore, also considering the ferroelastic distortion of the average lattice, the symmetry of the incommensurate phase is planar monoclinic $I2/m(\alpha 0\gamma)0s$.

The modulation vector suggested by the electron microscopy analysis was used to index the neutron diffraction pattern. All the observed satellite peaks can be indexed by this vector after refinement of the amplitude parameters (Fig. 4). The refined values of the four-dimensional metric of the lattice are summarized in Table 1. It is interesting to point out the excellent accuracy for characterizing the monoclinic distortion obtained thanks to the long wavelength and high resolution of the neutron powder diffractometer. The observed satellite reflections are compatible with the existence of the m_s glide mirror. Therefore, the refinement of the structure was performed according to the superspace group proposed by the electron microscopy analysis detailed above.

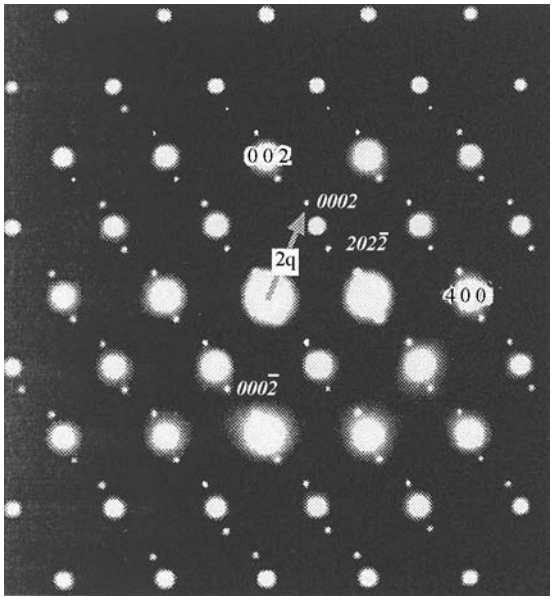

Figure 3
Electron diffraction pattern of a monodomain in the incommensurate phase along the $[010]_m$ zone axis. Two second-order satellite reflections are observed near the main spots. The systematic absences of odd-order satellites proves the existence of a four-dimensional glide plane m_s.

In a preliminary stage, only the average structure was refined, using anisotropic thermal displacement parameters for all atoms (Table 2). The solution has sketched out the amplitudes of the main components of the atomic modulated displacements. At this point, the thermal displacement parameters for all atoms were converted to isotropic and different combinations of sine and cosine waves with the estimated amplitudes were checked for consistency, comparing the observed and calculated diffraction patterns. Only the symmetry-allowed terms (summarized in Table 3) were considered.

In a following step, the thermal displacement parameters were also refined with the modulation terms. The thermal ellipsoids of all atoms were not significantly different from isotropic: for instance, the lead ellipsoid was $U^{11} = 0.024$ (5), $U^{22} = 0.023$ (1), $U^{33} = 0.024$ (1), $U^{13} = 0.000$ (1). These values confirm the absence of correlation between U^{22} and the main component of lead modulated displacement (along y). Therefore, the final results summarized in Table 4 are obtained using only isotropic thermal displacement parameters to describe the thermal factors of all atoms.

3.2. Atomic environment

The interatomic distances are summarized in Table 5. In the modulated phase there are two independent O atoms, each one corner-shared by the two types of octahedra: O1, sitting on the twofold axis and in the following referenced as the apical O atom, and O2, the oxygen atom defining the *basis* of the octahedra and therefore referenced as the basal O atom. The modulated displacements affecting these two atoms are sensibly different and four types of interatomic distances between nearest O atoms are of interest: between O1 and O2 in the Co and W octahedron, respectively, and between O2 atoms in the basal plane of the two octahedra. The plot of these distances against the four-dimensional coordinate t is displayed in Figs. 5 and 6. The effect of the modulated atomic displacements on the two octahedra are quite different: the W

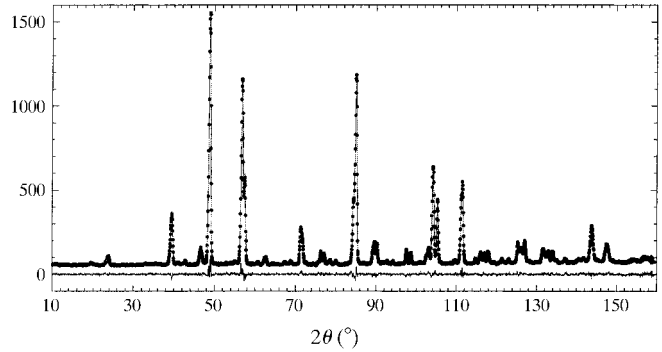

Figure 4
Observed (full dots), calculated and difference (solid lines) neutron diffraction patterns of Pb_2CoWO_6 in the incommensurate phase.

Table 4
Atomic positions and thermal parameters in the incommensurate structure at 250 K.

Some terms (*) allowed by the symmetry constraints are approximated to 0 when strongly correlated and are not significant.

Atom		B_0	A_1	B_1	A_2	B_2
O2	x	0.0203 (2)	0.0029 (9)	−0.0021 (6)	*	0.0079 (9)
	y	0.2428 (6)	−0.0024 (11)	−0.0180 (10)	*	0.003 (2)
	z	0.2382 (5)	0.0062 (13)	0.0156 (7)	0.0059 (18)	−0.0029 (18)
	u	0.0164 (5)				
O1	x	0.2399 (6)			*	0.005 (2)
	y	0	0.0130 (13)	−0.0144 (10)		
	z	−0.0392 (4)			−0.006 (3)	0.003 (3)
	u	0.0151 (7)				
Pb	x	0.2529 (7)			0.0034 (10)	−0.0013 (16)
	y	0	*	−0.0390 (7)		
	z	0.4984 (14)			*	−0.005 (2)
	u	0.0236 (4)				
Co	x	0.5			0.015 (4)	
	y	0	0.029 (4)			
	z	0			0.022 (6)	
	u	0.011 (3)				
W	x	0			0.002 (3)	
	y	0	−0.001 (2)			
	z	0			0.013 (4)	
	u	0.0052 (11)				

octahedron is very weakly affected by the modulation, exhibiting the whole bunch of interatomic distances between O atoms gathered in a narrow band centred at 2.75 Å; on the other hand, beside the obviously larger average value, the dispersion of distances is sensibly dilated in the Co octahedron. This seems to point to the concurrence of two effects: that the oxygen–oxygen interaction is sensibly stronger in the smaller octahedron and that the W—O bonds possess a greater stiffness than Co—O. This latter feature is confirmed by the smaller dispersion of the W—O bond lengths compared with Co—O, as summarized in Table 5.

The description of the bondings between Pb and O is less obvious. The 12 O neighbours are located at different distances ranging from 2.46 to 3.20 Å. If we focus our attention on the shorter bondings (Fig. 7), it is interesting to observe that at almost any t value, four short distances of less than 2.75 Å are formed. Two are with basal and two with apical O atoms. One of the two bondings with an apical oxygen is maintained whatever the cell in the crystal. The three other bondings change in different cells of the crystal. In some sections of the crystal, a fifth short Pb—O bonding occurs. Therefore, the lead coordination topology undergoes substantial changes in different cells of the crystal. The observed configuration of the four shortest bondings between lead and oxygen ranges from distorted pyramidal (a configuration rather close to that in massicot, although involving rather longer bond lengths) to almost tetrahedral. Nevertheless, these large variations are partly tempered by the existence of the other short bondings, leading to a more regular behaviour of the coordination in the different cells of the crystal. This particular behaviour witnesses an adaptative character of lead bondings to fit the distorted oxygen framework.

It is interesting to point out that, for a given Pb atom, no bonding at less than 3.00 Å occurs with the apical oxygen opposite to the always bonded one (see Fig. 8). This fact gives rise to an interesting oscillating behaviour for Pb displacements: Pb atoms describe in t-space a pendular movement,

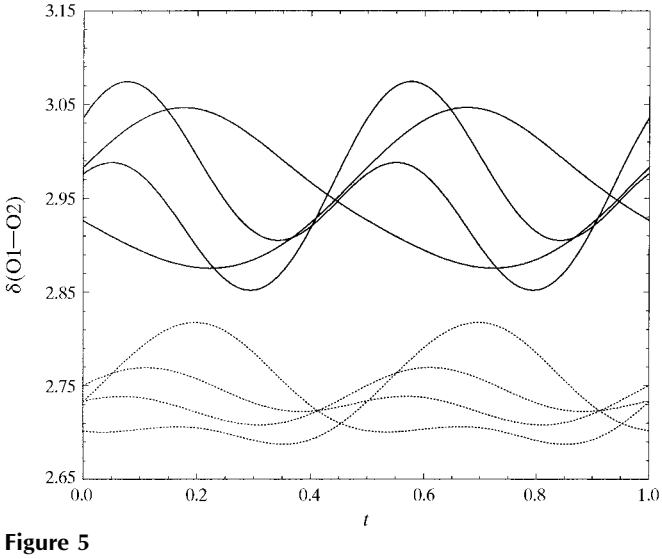

Figure 5
Interatomic distances between O1 (apical) and the nearest-neighbour O2 atoms (sitting in 100). The solid lines represent distances in the Co octahedron, the dotted lines distances in the W octahedron.

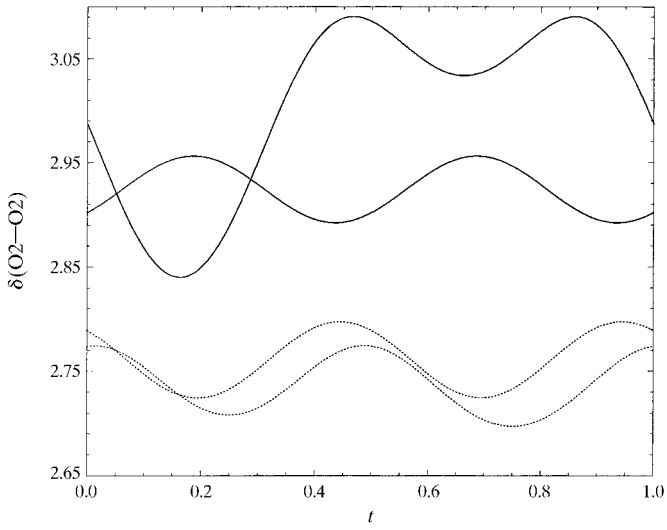

Figure 6
Interatomic distances between O2 atoms belonging to the Co octahedron (solid lines) and W octahedron (dotted lines).

Table 5
Bond lengths (Å) for the incommensurate structure.

	No.	Mean (Å)	Min. (Å)	Max. (Å)
Pb—O1	4	2.851	2.533	3.163
Pb—O2	8	2.837	2.457	3.204
W—O1	2	1.924	1.877	1.972
W—O2	4	1.944	1.896	1.974
Co—O1	2	2.091	1.959	2.223
Co—O2	4	2.102	1.952	2.242

mainly along the *y* direction, around the apical oxygen bonded in all *t*-sections: this complex trajectory is actually responsible for the alternating configurations of the shortest bonds to O neighbours.

4. Discussion

It is instructive to compare this structural resolution to that for a single crystal (Bonin *et al.*, 1995). Lead cobalt tungstate displays a complex ferroelastic domain state in the incommensurate phase. Therefore, solving the structure using single-crystal methods is very complex (Bonin *et al.*, 1995): since main and satellite reflections can totally or partly overlap, the treatment of domains is added to the usual complexity of solving a modulated phase. In this framework, working out a reliable solution is very difficult, because an accurate repartition of the intensities of different domains and the effects of coherence and antiphase boundaries are difficult to model. In that work, different space groups were checked and the correct choice was not obvious, since the sample was in a polydomain state. The existence of domains with different orientations induced some ambiguities in the definite choice of the metrics and the symmetry operators, and it was resolved considering the most simple model of displacive modulation. Nevertheless, in that space group (that is the only superspace group compatible with our powder diffraction data and electron microscopy), the anisotropic thermal displacement parameters of lead remained abnormally large in the *z* direction, although no modulated displacement was expected along this direction. This effect is probably related to the correlation between the refined twin volume ratios and the population parameters (Bonin *et al.*, 1995). Only a schematic description of the modulation was possible from the refinement of the single-crystal structure. Restraining the refinement of atomic modulated displacements to first-order harmonics smooths the description of the B cations and lead complex coordination. If, among the different solutions proposed by Bonin *et al.*, the monoclinic $I2/m(\alpha 0\gamma)0s$ structure is considered, the structure they propose is, to a given extent, a constrained average of the structure determined in this work.

Powder refinements are generally less useful than single-crystal ones since the three-dimensional information contained in the reciprocal lattice is reduced to a one-dimensional diffraction pattern. This limit turns into an advantage when treating polydomain phases since the repartition of different orientation domain intensities can be handled using statistical weights. Furthermore, in Rietveld refinements, the existence of a whole pattern profile allows an accurate extraction of very weak intensities, sometimes very useful for stabilizing the Fourier expansion used to describe the modulated atomic displacements.

One more advantage in the present case is the use of neutron scattering: in fact, the modulated displacements in the present structure involve heavy scatterers as lead (in the X-ray sense) and light ones (always in the X-ray perspective) as

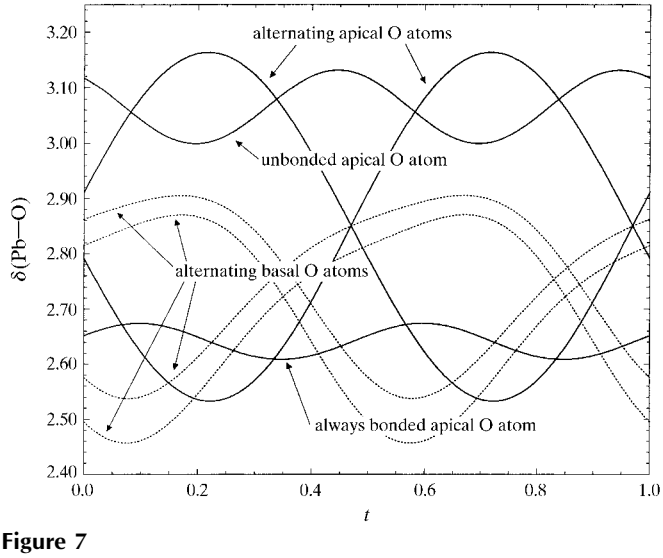

Figure 7
Selection of bond lengths between Pb and nearest O atoms (solid lines for Pb—O1, dotted for Pb—O2). The remaining four bond lengths between Pb and basal O atoms are always longer than 2.8 Å.

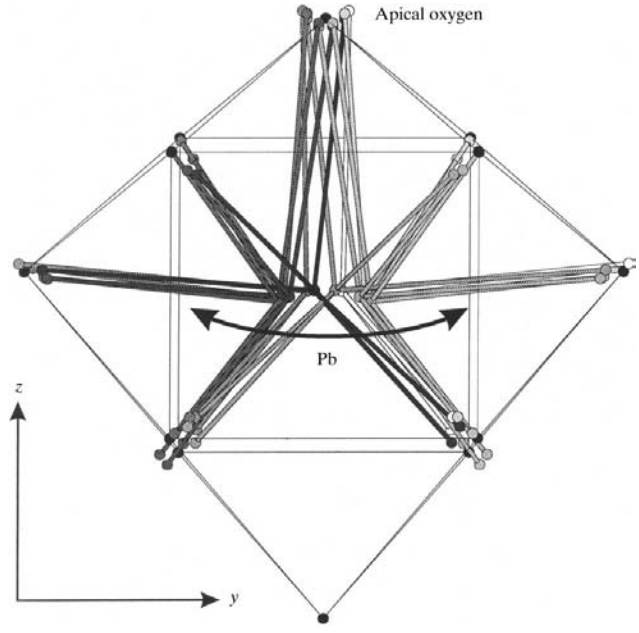

Figure 8
Schematic representation of Pb—O bondings in the crystal at various *t* outlining the pendular behaviour of a short bond with an apical O atom. The short bonds at less than 2.75 Å are displayed on a grey scale from light to dark grey when *t* increases from 0 to 1.

oxygen. Since all the structural components in the structure present similar neutron scattering lengths, starting the refinement is somewhat harder, but there will be no strong bias and a great accuracy is in principle possible for all modulation waves.

It is interesting to point out that second-order satellites, missing in the single-crystal data collection, are observed on the neutron powder diffraction pattern, allowing an easy phasing and refinement of the corresponding second-order Fourier terms: the reliability factor for these weak peaks can be judged satisfactory. The inclusion of these terms in the refinement allows a smoother behaviour for the shortest bondings and a more satisfactory description of the structure. All these reasons suggest that the refinement of powder diffraction data can be considered more satisfactory since there is no need to introduce anisotropic thermal ellipsoids and the modulated displacements describe well all the experimental nuclear density.

The refinement of neutron powder diffraction data of lead cobalt tungstate has allowed an accurate description of the modulated displacements of the oxygen framework and of the cations. The main effect of the modulation is to modify the antiparallel shifts of lead atoms and oxygen octahedron tilts. In particular, the octahedron tilt can be decomposed in an almost non-modulated tilt around $[010]_m$ and a modulated tilt around $[100]_m$. The incommensurability of the phase witnesses a possible competing interaction between the dipolar interactions arising from these atomic displacements and the elastic deformation of the lattice.

It is a pleasure to aknowledge Dr Jean-François Bérar for the valuable discussions during the development of the program modules for the handling of modulated structures now included in the refinement code *XND*.

References

Baldinozzi, G., Sciau, P. & Buffat, P. A. (1993). *Solid State Commun.* **86**, 541–544.
Baldinozzi, G., Sciau, P. & Bulou, A. (1995). *J. Phys. Condens. Matter*, **7**, 8109–8117.
Bérar, J. F. & Garnier, P. (1992). *APD 2nd Conference, NIST*. Special publication 846, p. 212. NIST, 100 Bureau Drive, Gaithersburg, MD 20899, USA.
Bonin, M., Paciorek, W., Schenk, K. J. & Chapuis, G. (1995). *Acta Cryst.* B**51**, 48–54.
Brixel, W., Werk, M. L., Fischer, P., Bührer, W., Rivera, J. P., Tissot, P. & Schmid, H. (1985). *Jpn. J. Appl. Phys.* Suppl. **24–2**, 242–244.
Lines, M. E. (1996). *Principles and Applications of Ferroelectric and Related Materials.* Oxford University Press.
Petříček, V. & Dusek, M. (1998). *Jana98 User's Manual.* Institute of Physics, Academy of Sciences of the Czech Republic, Na Slovance 2, 182 21 Prague.
Sciau, P., Calvarin, G., Sun, B. N. & Schmid, H. (1992). *Phys. Status Solidus A*, **129**, 309–321.
Sciau, P. & Grebille, D. (1994). *Aperiodic*94. World Scientific.
Sciau, P., Krusche, K., Buffat, P. A. & Schmid, H. (1990). *Ferroelectrics*, **107**, 235–240.
Sun, B. N., Boutellier, R., Sciau, P., Burkhardt, E., Rodriguez, V. & Schmid, H. (1991). *J. Cryst. Growth*, **112**, 71–83.
Wilson, A. J. C. (1992). *International Tables for Crystallography*, Vol. C. Dordrecht: Kluwer Academic Publishers.